Ollila, Esa

Greedy Capon Beamformer

Published in:
IEEE Signal Processing Letters

DOI:
10.1109/LSP.2024.3475351

Published: 01/01/2024

Document Version
Publisher's PDF, also known as Version of record

Greedy Capon Beamformer

Esa Ollila, *Senior Member, IEEE*

***Abstract*—We propose greedy Capon beamformer (GCB) for direction finding of narrow-band sources present in the array's viewing field. After defining the grid covering the location search space, the algorithm greedily builds the interference-plus-noise covariance matrix by identifying a high-power source on the grid using Capon's principle of maximizing the signal to interference plus noise ratio while enforcing unit gain towards the signal of interest. An estimate of the power of the detected source is derived by exploiting the unit power constraint, which subsequently allows to update the noise covariance matrix by simple rank-1 matrix addition composed of outerproduct of the selected steering matrix with itself scaled by the signal power estimate. Our numerical examples demonstrate effectiveness of the proposed GCB in direction finding where it performs favourably compared to the state-of-the-art algorithms under a broad variety of settings. Furthermore, GCB estimates of direction-of-arrivals (DOAs) are very fast to compute.**

***Index Terms*—Beamforming, MVDR beamforming, direction finding, source localization, greedy pursuit.**

I. Introduction

COMMON to most direction finding (DF) methods is the need to estimate the unknown $N \times N$ array covariance matrix $\mathbf{\Sigma} = \mathrm{cov}(\mathbf{x}) \succ 0$ of the array output $\mathbf{x} \in \mathbb{C}^N$ of N-sensors. For example, the conventional beamformer [1] and the standard Capon beamformer (SCB) [2] require an estimate of $\mathbf{\Sigma}$ to measure the power of the beamformer output as a function of the direction-of-arrival (DOA). In addition, many high-resolution subspace-based DOA algorithms (such as MUSIC [3] or R(oot)-MUSIC [4]) compute the noise or signal subspaces from the eigenvectors of the array covariance matrix. Array covariance matrix is conventionally estimated from the array snapshots via the sample covariance matrix (SCM). However, the SCM is poorly estimated when the snapshot size is small and adaptive beamformers (such as SCB) are not computable when $L < N$. Sparse methods for DOA estimation [5] provide a remedy for these issues.

We assume that K narrowband sources are present in the array's viewing field. Let $\mathbf{a}(\theta) \in \mathbb{C}^N$ denote the array manifold, where θ denotes the generic location parameter in the location space Θ. For example, $\mathbf{a}(\theta) = \left(1, e^{-\jmath \cdot 1 \cdot \frac{2\pi d}{\lambda} \sin\theta}, \ldots, e^{-\jmath \cdot (N-1) \cdot \frac{2\pi d}{\lambda} \sin\theta}\right)^\top$ for Uniform Linear Array (ULA), where λ is the wavelength, d is the element spacing between the sensors and $\theta \in \Theta = [-\pi/2, \pi/2)$ is the DOA in radians. For an arbitrary steering vector in the array manifold we use notation $\mathbf{a}$, dropping the dependency on θ. The output of a beamformer is defined by $y = \mathbf{w}^{\mathsf{H}}\mathbf{x}$, where $\mathbf{w}$ is the beamformer weight vector that depends on θ through $\mathbf{a}$. Ideally, the beamformer weight $\mathbf{w} = \mathbf{w}(\theta)$ is chosen such that the beamformer will null the interferences and noise while allowing the signal of interest (SOI) at θ to pass undistorted. A beamformer estimates the locations of the K signals impinging on the array as K peaks in the array output power distribution [1], [6], [7]:

$$P(\theta) = \mathbb{E}\left[|\mathbf{w}^{\mathsf{H}}\mathbf{x}|^2\right] = \mathbf{w}^{\mathsf{H}}\mathbf{\Sigma}\mathbf{w}$$

using a fine grid $\{\theta_m\}_{m=1}^M$ covering Θ, i.e., allowing θ (and hence $\mathbf{a}$ in the design of the beamformer weight $\mathbf{w}$) vary through the location space Θ.

As sparse DOA methods leverage the covariance matrix's geometry, they often outperform traditional approaches in low sample size (LSS) scenarios. Diagonal loading of the SCM is another common method to combat LSS settings [8], [9], [10], [11], [12], but these methods often involve increased computational complexity arising from determining the optimal loading factor. In this letter, we propose a greedy Capon beamformer (GCB) that greedily selects the next high-power source (not yet detected) using Capon beamforming principle and subsequently updates the interference-plus-noise covariance matrix (INCM). Although GCB may seem heuristic, it is yet logical and follows generic greedy selection algorithmic framework. The approach is computationally light; it does not require computing the eigenvalue decomposition as needed by MUSIC or R-MUSIC nor inverting the SCM as in SCB (i.e., $L > N$ is not required). There are similar sparsity and covariance based DOA estimation methods, e.g, [13], [14], [15], [16], [17], [18], [19], [20]. or review in [5], which are primarily iterative algorithms constructed using some optimization principles. Our simulation studies illustrate that the proposed GCB performs favourably against SCB and state-of-the-art (SOTA) methods.

II. Capon Beamformer

Let the $N \times N$ array covariance matrix $\mathbf{\Sigma}$ be decomposed as

$$\mathbf{\Sigma} = \gamma \mathbf{a}\mathbf{a}^{\mathsf{H}} + \mathbf{Q} \tag{1}$$

where $\gamma > 0$ denotes the power of the SOI, $\mathbf{a} \in \mathbb{C}^N$ is the array steering vector of the SOI at θ, and $\mathbf{Q}$ is an $N \times N$ positive definite ($\mathbf{Q} \succ 0$) INCM. It is assumed that the noise is spatially white and $K-1$ uncorrelated directional interfering signals are

Received 1 August 2024; revised 19 September 2024; accepted 23 September 2024. Date of publication 7 October 2024; date of current version 14 October 2024. This work was supported by the Research Council of Finland under Grant 359848. The associate editor coordinating the review of this article and approving it for publication was Prof. Huseyin Hacihabiboglu.

The author is with the Department of Information and Communications Engineering, Aalto University, FI-00076 Aalto, Finland (e-mail: esa.ollila@aalto.fi).

Digital Object Identifier 10.1109/LSP.2024.3475351

present. Then the matrix $\mathbf{Q}$ can be expressed in the form

$$\mathbf{Q} = \sum_{k=2}^{K} \gamma_k \mathbf{a}_k \mathbf{a}_k^{\mathsf{H}} + \sigma^2 \mathbf{I}$$

where $\sigma^2\mathbf{I}$ is an $N \times N$ noise covariance matrix (i.e., we assume spatially white noise), $\mathbf{a}_k = \mathbf{a}(\theta_k) \in \mathbb{C}^N$ is the steering vector of the directional interference signal at θ_k, and $\gamma_k > 0$ is the associated signal power ($k = 2, \ldots, K$). Without any loss of generality (w.l.o.g.) we will assume that all steering vectors are normalized such that $\|\mathbf{a}_k\|^2 = N$ holds.

Capon Beamformer (CB) minimizes the array output power subject to the constraint that the SOI is passed undistorted:

$$\min_{\mathbf{w}} \mathbf{w}^{\mathsf{H}} \boldsymbol{\Sigma} \mathbf{w} \quad \text{subject to } \mathbf{w}^{\mathsf{H}} \mathbf{a} = 1, \qquad \text{(P1)}$$

or equivalently, maximizes the signal to interference plus noise ratio (SINR) at its output while enforcing a unit gain towards the SOI:

$$\max_{\mathbf{w}} \frac{\gamma |\mathbf{w}^{\mathsf{H}} \mathbf{a}|^2}{\mathbf{w}^{\mathsf{H}} \mathbf{Q} \mathbf{w}} \quad \text{subject to } \mathbf{w}^{\mathsf{H}} \mathbf{a} = 1. \qquad \text{(P2)}$$

Due to the first formulation (P1), CB is also often called minimum variance distortionless response (MVDR) beamformer. The solutions to power minimization problem (P1) and SINR maximization (P2) are equivalent [21] and the optimum beamformer weight for both problems is given by

$$\mathbf{w}_{\text{opt}} = \frac{\boldsymbol{\Sigma}^{-1}\mathbf{a}}{\mathbf{a}^{\mathsf{H}}\boldsymbol{\Sigma}^{-1}\mathbf{a}} = \frac{\mathbf{Q}^{-1}\mathbf{a}}{\mathbf{a}^{\mathsf{H}}\mathbf{Q}^{-1}\mathbf{a}}. \qquad (2)$$

The optimal power and SINR are then

$$P_{\text{opt}} = \mathbb{E}\left[|\mathbf{w}_{\text{opt}}^{\mathsf{H}}\mathbf{x}|^2\right] = \mathbf{w}_{\text{opt}}^{\mathsf{H}}\boldsymbol{\Sigma}\mathbf{w}_{\text{opt}} = \frac{1}{\mathbf{a}^{\mathsf{H}}\boldsymbol{\Sigma}^{-1}\mathbf{a}}, \qquad (3)$$

$$\text{SINR}_{\text{opt}} = \frac{\gamma |\mathbf{w}_{\text{opt}}^{\mathsf{H}}\mathbf{a}|^2}{\mathbf{w}_{\text{opt}}^{\mathsf{H}}\mathbf{Q}\mathbf{w}_{\text{opt}}} = \gamma \mathbf{a}^{\mathsf{H}}\mathbf{Q}^{-1}\mathbf{a}. \qquad (4)$$

So far we have discussed the ideal situation, so assuming that θ of SOI (and hence the steering vector $\mathbf{a}$) as well as the covariance matrix $\boldsymbol{\Sigma}$ are known exactly. Since $\boldsymbol{\Sigma}$ is unavailable in practise, it is commonly estimated by the SCM $\hat{\boldsymbol{\Sigma}} = \frac{1}{L}\sum_{l=1}^{L} \mathbf{x}_l \mathbf{x}_l^{\mathsf{H}} \in \mathbb{C}^{N\times N}$, where $\mathbf{x}_l \in \mathbb{C}^N$ represents the l^{th} snapshot and L denotes the number of snapshots (i.e., sample size). Consider a grid $\{\theta\}_{m=1}^{M}$, $\theta_1 < \ldots < \theta_M$, of location parameters covering Θ, and let $\{\mathbf{a}_m\}_{m=1}^{M}$ denote the corresponding steering vectors. Write $\boldsymbol{\theta} = (\theta_1, \ldots, \theta_M)^{\top}$ for the M-vector of DOA parameters on the grid. Then SCB computes an estimate of the spatial power for SOI at θ_i using $\hat{P}_{\text{SCB},i} = \left(\mathbf{a}_i^{\mathsf{H}}\hat{\boldsymbol{\Sigma}}^{-1}\mathbf{a}_i\right)^{-1}$, $i = 1, \ldots, M$ which is an empirical (sample based) estimate of (3). Typically, it is assumed that the grid resolution is fine enough so that the true location parameters of the sources lie in close proximity to the grid. SCB then identifies the indices of the largest K peaks in the spatial spectrum:

$$\mathcal{K} = \mathsf{findpeaks}_K(\hat{P}_{\text{SCB},1}, \ldots, \hat{P}_{\text{SCB},M})$$

where $\mathcal{K} \subset \{1, \ldots, M\}$ with $|\mathcal{K}| = K$ and outputs the vector of K DOA estimates as $\hat{\boldsymbol{\theta}} = \boldsymbol{\theta}_{\mathcal{K}}$, where $\boldsymbol{\theta}_{\mathcal{K}}$ denotes a K-vector consisting of components of an M-vector $\boldsymbol{\theta}$ corresponding to indices in the set $\mathcal{K}$.

III. The Greedy Capon Beamformer

First we prove a result that relates the power γ of the SOI to the optimum power and optimum SINR of CB.

Lemma 1: The power γ of the SOI at steering vector $\mathbf{a}$ is given by

$$\gamma = \mathbf{w}_{\text{opt}}^{\mathsf{H}} (\boldsymbol{\Sigma} - \mathbf{Q}) \mathbf{w}_{\text{opt}} = P_{\text{opt}} - \left(\mathbf{a}^{\mathsf{H}}\mathbf{Q}^{-1}\mathbf{a}\right)^{-1} \qquad (5)$$

where P_{opt} is the optimum beamformer power (3).

Proof: Due to unit gain constraint one has that $\mathbf{w}_{\text{opt}}^{\mathsf{H}}\mathbf{a} = 1$ and since $\gamma\mathbf{a}\mathbf{a}^{\mathsf{H}} = \boldsymbol{\Sigma} - \mathbf{Q}$ from (1), we may write

$$\gamma = \gamma |\mathbf{w}_{\text{opt}}^{\mathsf{H}}\mathbf{a}|^2 = \mathbf{w}_{\text{opt}}^{\mathsf{H}}(\gamma\mathbf{a}\mathbf{a}^{\mathsf{H}})\mathbf{w}_{\text{opt}} = \mathbf{w}_{\text{opt}}^{\mathsf{H}}(\boldsymbol{\Sigma} - \mathbf{Q})\mathbf{w}_{\text{opt}}$$

$$= \mathbf{w}_{\text{opt}}^{\mathsf{H}}\boldsymbol{\Sigma}\mathbf{w}_{\text{opt}} - \mathbf{w}_{\text{opt}}^{\mathsf{H}}\mathbf{Q}\mathbf{w}_{\text{opt}} = P_{\text{opt}} - \left(\mathbf{a}^{\mathsf{H}}\mathbf{Q}^{-1}\mathbf{a}\right)^{-1} \qquad (6)$$

where the last identity follows by recalling (3) and noting that $\mathbf{w}_{\text{opt}}^{\mathsf{H}}\mathbf{Q}\mathbf{w}_{\text{opt}} = (\mathbf{a}^{\mathsf{H}}\mathbf{Q}^{-1}\mathbf{a})^{-1} = (\text{SINR}_{\text{opt}}/\gamma)^{-1}$, when the latter form of $\mathbf{w}_{\text{opt}}$ in (2) is invoked. □

Lemma 1 also illustrates P_{opt} is essentially equal to the power γ of the SOI in ideal conditions. Namely, if the INCM $\mathbf{Q}$ contains only the white noise term, i.e., $\mathbf{Q} = \sigma^2\mathbf{I}$, then $\gamma = P_{\text{opt}} - \frac{\sigma^2}{N}$ where we used that $\mathbf{a}^{\mathsf{H}}\mathbf{a} = N$. If $\gamma \gg \sigma^2$ and N is reasonably large, then we can notice that $\gamma \approx P_{\text{opt}}$ which is an expected result.

Lemma 1 will now be used in our greedy Capon beamformer (GCB) algorithm to estimate the power of the detected signal. GCB greedily builds the INCM $\mathbf{Q}$ by identifying a high-power source on the grid using Capon's principle of maximizing the SINR while enforcing unit gain towards the SOI. The **GCB algorithm** proceeds as follows:

Input: The SCM $\hat{\boldsymbol{\Sigma}}$, the number of sources K, the grid of DOAs $\boldsymbol{\theta} = (\theta, \ldots, \theta_M)^{\top}$ and the steering vectors $\mathbf{a}_1, \ldots, \mathbf{a}_M$.

Initialize: Set $\hat{\mathbf{Q}} = [\text{tr}\left(\hat{\boldsymbol{\Sigma}}\right)/N] \cdot \mathbf{I}$ and $\mathcal{M} = \emptyset$. Initially, the set $\mathcal{M}$, which gathers the identified sources, is empty, and the INCM $\hat{\mathbf{Q}}$ is merely an estimate of the white noise matrix $\sigma^2\mathbf{I}$.

Main iteration: for $k = 1, \ldots, K$, iterate the steps below

1) Compute the beamformer output power estimates

$$\hat{P}_i = \mathbf{w}_i^{\mathsf{H}}\hat{\boldsymbol{\Sigma}}\mathbf{w}_i = \frac{\mathbf{a}_i^{\mathsf{H}}\hat{\mathbf{Q}}^{-1}\hat{\boldsymbol{\Sigma}}\hat{\mathbf{Q}}^{-1}\mathbf{a}_i}{\left(\mathbf{a}_i^{\mathsf{H}}\hat{\mathbf{Q}}^{-1}\mathbf{a}_i\right)^2}, \; i = 1, \ldots, M,$$

where $\mathbf{w}_i = \hat{\mathbf{Q}}^{-1}\mathbf{a}_i / \left(\mathbf{a}_i^{\mathsf{H}}\hat{\mathbf{Q}}^{-1}\mathbf{a}_i\right)$ signifies the beamformer weight for location θ_i on the grid.

2) Identify the indices of the k largest peaks in the spatial spectrum:

$$\mathcal{K} = \mathsf{findpeaks}_k\left(\hat{P}_1, \ldots, \hat{P}_M\right),$$

i.e., $\mathcal{K} \subset \{1, \ldots, M\}$ with cardinality $|\mathcal{K}| = k$.

3) If $k < K$, then execute steps 4) – 7).

4) Choose the index that has the least coherence with steering vectors that have been picked up so far:

$$i_k = \arg\min_{i\in\mathcal{K}} \left(\max_{j\in\mathcal{M}} |\mathbf{a}_i^{\mathsf{H}}\mathbf{a}_j|\right).$$

TABLE I
AVERAGE RUNNING TIMES OF METHODS ON A LAPTOP

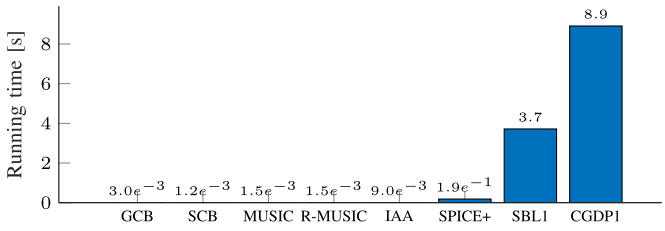

Thus, i_k is the index from the set $\mathcal{K}$ corresponding to the steering vector $\mathbf{a}_{i_k}$, which is the least coherent with the previously selected steering vectors $\mathbf{a}_j$ for $j \in \mathcal{M}$.

5) Update the set $\mathcal{M} \leftarrow \mathcal{M} \cup \{i_k\}$ of chosen indices.
6) Estimate the signal power of the chosen source as $\hat{\gamma}_k = \hat{P}_{i_k} - \left(\mathbf{a}_{i_k}^{\mathsf{H}} \hat{\mathbf{Q}}^{-1} \mathbf{a}_{i_k}\right)^{-1}$, i.e., using (5) of Lemma 1.
7) Update the INCM as $\hat{\mathbf{Q}} \leftarrow \hat{\mathbf{Q}} + \hat{\gamma}_k \mathbf{a}_{i_k} \mathbf{a}_{i_k}^{\mathsf{H}}$. Such rank-1 update allows to compute the inverse covariance matrix $\hat{\mathbf{Q}}^{-1}$ efficiently using the Sherman-Morrison [22] formula, yielding

$$\hat{\mathbf{Q}}^{-1} \leftarrow \hat{\mathbf{Q}}^{-1} - \frac{\hat{\gamma}_k \hat{\mathbf{Q}}^{-1} \mathbf{a}_{i_k} \mathbf{a}_{i_k}^{\mathsf{H}} \hat{\mathbf{Q}}^{-1}}{1 + \hat{\gamma}_k \mathbf{a}_{i_k}^{\mathsf{H}} \hat{\mathbf{Q}}^{-1} \mathbf{a}_{i_k}}. \tag{7}$$

Output: After K iterations, the DOA estimates are given as $\hat{\boldsymbol{\theta}} = \boldsymbol{\theta}_{\mathcal{K}}$ similarly as in the SCB algorithm outlined in Section II.

MATLAB and python functions, and simulation implementations, are available at https://github.com/esollila/GCB.

The dominant complexity of GCB algorithm is in the matrix-vector multiplications of step 1, whose complexity is $O(N^2)$. This is repeated for all M steering vectors, so total complexity is $O(MN^2)$. The complexity of step 4 is $O(k^2 N)$, where $k < K$ while the complexity of the peak finding algorithm in step 2 is $O(M)$. The complexity of rank-one update in step 7 is only $O(N^2)$ instead of $O(N^3)$ due to inverting an $N \times N$ matrix. Hence the overall complexity of GCB algorithm is $O(KMN^2)$. The complexity of SCB and MUSIC is $O(MN^2 + N^3)$ which is typically slightly better than that of GCB since their complexity reduces to $O(MN^2)$ when $M \gg N$. However, both the SCB and MUSIC need to assume $L > N$ which is not needed by GCB. The computational complexity of IAA(-APES) [15, Table 2], a widely used sparse DOA estimation method, is $O(N_{iter}(2MN^2 + N^3))$, where N_{iter} denotes the number of iterations required for convergence. This complexity is generally higher than that of GCB, but similar magnitude when $N_{iter} < N \ll M$.

Average running times of different methods on a MacBook Pro M3 laptop in the simulation set-up of Section IV ($K = 4$, $N = 20$, $M = 1801$, $L = 125$) are compared in Table I. Running times are averages over 100 MC simulations and over different SNR levels of Fig. 1. We compared with the following SOTA methods: IAA, SPICE+ [14, eq. (44)–(46)], SBL1 [17, Table 1] and CGDP(-SBL)1 [20, Table I]. For the last two methods, we used the efficient implementations available at the authors github pages [23], [24] while for IAA and SPICE+, we used our own implementation. As can be noted, CGBD1 and SBL1 are 3 orders (while SPICE+ 2 orders) of magnitude slower than GCB, SCB, MUSIC, R-MUSIC, and IAA, i.e., taking seconds instead of milliseconds to compute.

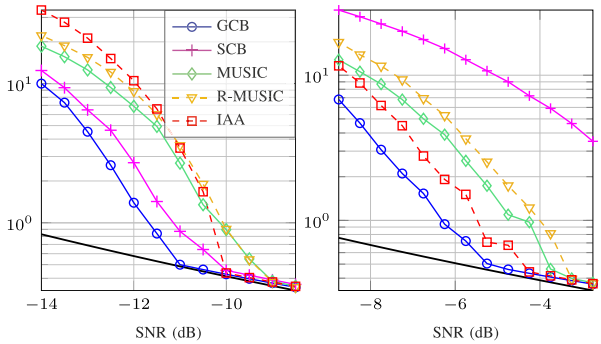

Fig. 1. RMSE of $\hat{\boldsymbol{\theta}}$ (deg.) versus SNR when $L = 125$ (left panel) and $L = 25$ (right panel); $K = 4$, $N = 20$, $M = 1801$.

Another advantage of GCB over SCB is its robustness to coherent sources. While coherent sources make the SCM poorly conditioned, the GCB estimate of the INCM $\mathbf{Q}$ remains well-conditioned, eliminating the need for mitigation techniques like spatial smoothing.

IV. SIMULATION STUDY

The array is ULA with half a wavelength inter-element spacing and number of sensors is $N = 20$. The grid size is $M = 1801$, and spacing is uniform, thus providing angular resolution $\Delta\theta = 0.1^o$. The number of Monte-Carlo (MC) trials is 15000 in order to obtain accurate finite sample performance and smooth curves. The SNR of k^{th} source is defined as $\text{SNR}_k = \gamma_k/\sigma^2$, where γ_k is the signal power of the k^{th} source and $\sigma^2 > 0$ is the noise variance. The array SNR is defined as average SNR (dB) $= \frac{10}{K}\sum_{k=1}^{K} \log_{10} \text{SNR}_k$. The K sources are following complex circular Gaussian distribution, $s_k \sim \mathcal{CN}(0, \gamma_k)$, $k = 1, \ldots, K$, unless otherwise noted.

We compare the proposed GCB method against the Cramér-Rao lower bound (CRLB) [1, Ch. 8.4.2], SCB, MUSIC R-MUSIC, and IAA which were chosen as they share similar computational complexity (*cf.* Table I). All methods, except R-MUSIC, use a grid of DOAs that sets the angular resolution limit of the technique. In our set-up we have $K = 4$ sources at DOAs $\theta_1 = -30.1^o$, $\theta_2 = -20.02^o$, $\theta_3 = -10.02^o$ and $\theta_4 = 3.02^o$, i.e., all except the 1^{st} source is off the predefined grid. The SNR of the last 3 sources are -1, -2 and -5 dB relative to the 1^{st} source. The DOA estimates $\hat{\theta}_1, \ldots, \hat{\theta}_4$ are ordered by finding the nearest neighbor first for the largest magnitude source θ_1, then for θ_2, followed by θ_3 and the remaining DOA estimate is paired with smallest magnitude source θ_4. We then calculated the empirical root mean squared error (RMSE) $\|\hat{\boldsymbol{\theta}} - \boldsymbol{\theta}\|$ averaged over all MC trials. We also calculated RMSE for each source $|\hat{\theta}_i - \theta_i|$.

RMSE versus SNR: Fig. 1 displays the performance when the sample size is $L = 125$ (left panel) and $L = 25$ (right panel) and SNR varies. The proposed GCB exhibits the best performance across all SNR levels and each sample length L. At low sample size ($L = 25$), the second-best performing methods is IAA but its performance deteriorates and is similar to MUSIC and

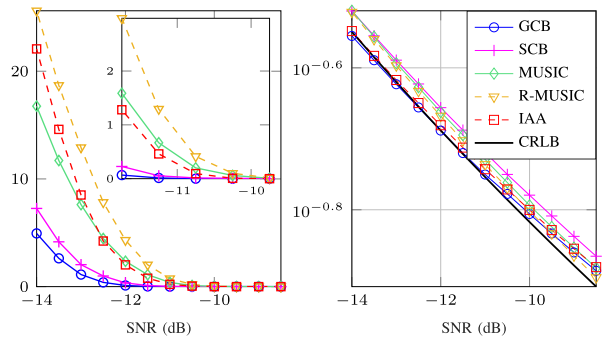

(a) percentage of misdetection (b) RMSE of $\hat{\theta}_1$

Fig. 2. (a) percentage of misdetection vs SNR; (b) RMSE of $\hat{\theta}_1$ (deg.) versus SNR; $K = 4$, $L = 125$, $N = 20$, $M = 1801$.

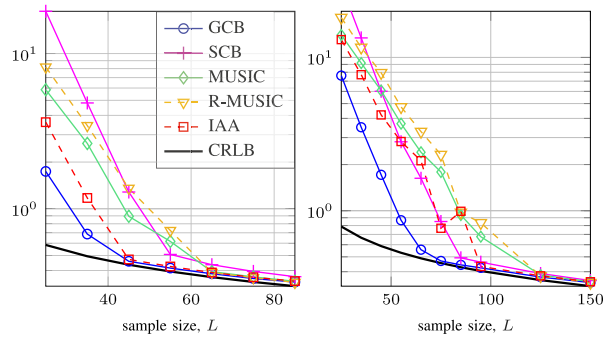

Fig. 3. RMSE of $\hat{\boldsymbol{\theta}}$ (deg.) versus sample size L when SNR is -7 dB (left panel) and -9 dB (right panel); $K = 4$, $N = 20$, $M = 1801$.

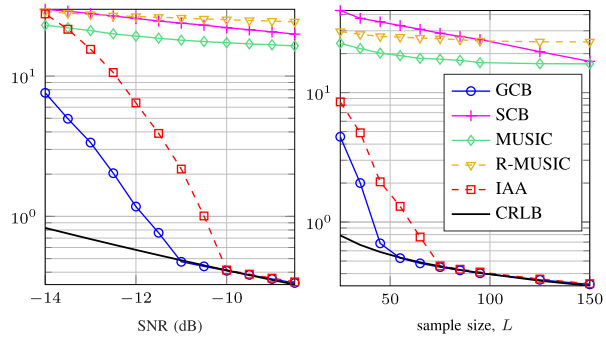

Fig. 4. Correlated constant modulus sources scenario. Left: RMSE versus SNR when sample size is $L = 125$. Right: RMSE versus sample size L when SNR is -9dB; $K = 4$, $N = 20$, $M = 1801$.

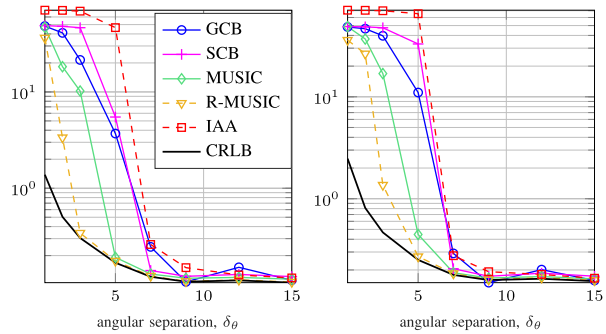

Fig. 5. RMSE of $\hat{\boldsymbol{\theta}}$ (deg.) versus $\delta_\theta = \theta_2 - \theta_1$ in two source scenario when SNR is -6 dB (left panel) and -3 dB (right panel); $K = 2$, $N = 20$, $M = 1801$, $\theta_1 = -30.02^o$.

R-MUSIC when $L = 125$. Additionally, note that for $L = 25$, SCB and GCB exhibit opposite performances: SCB performs the worst among all methods, while GCB achieves the best results. This highlights GCB's high robustness to low sample sizes. At very low SNR, the proposed GCB has superior performance. For example, at SNR of -11 dB and $L = 125$, GCB has one order of magnitude smaller RMSE than IAA.

Percentage of misdetection: The main challenge in low SNR conditions is accurately estimating the 4^{th} source, which has the lowest power. We say that misdetection (MD) occurs when a DOA estimation error exceeds a threshold $\tau = \min_{i\neq j} \frac{1}{2}|\theta_i - \theta_j|$. We compute MD using formula $\text{MD} = I(\max_i |\hat{\theta}_{(i)} - \theta_i| > \tau)$, where $\hat{\theta}_{(i)}$ are the ordered DOA estimates ($\hat{\theta}_{(1)} < \ldots < \hat{\theta}_{(4)}$) and $I(\cdot)$ denotes the indicator function. Fig. 2(a) shows the misdetection rate versus SNR for $L = 125$. The figure highlights the poor performance of MUSIC and R-MUSIC in low SNR conditions. This is further confirmed in Fig. 2(b) which displays the RMSE of the first (highest power) DOA estimate $\hat{\theta}_1$. As can be noted, all methods perform more similarly in estimating θ_1.

RMSE versus sample size L: Fig. 3 shows the RMSE versus sample size L at SNR -7 dB (left panel) and -9 dB (right panel). GCB consistently exhibits the best performance across all L values. MUSIC and R-MUSIC catch up a bit with sparsity based GCB and IAA methods when L increases. Additionally, also SCB outperforms MUSIC and R-MUSIC when SNR is -9 dB.

Coherent sources scenario: We generate non-Gaussian sources with constant modulus by generating the k^{th} source as $s_k = \gamma_k \exp(\jmath\vartheta_k)$ where the phases ϑ_k, $k = 1, \ldots, K$ are independently and uniformly distributed in $[0, 2\pi)$ while γ_k are as earlier. We set $\vartheta_1 = \vartheta_4$, i.e., source 1 and source 4 have identical phases, and are thus fully coherent. We repeated previous simulation studies and display the RMSE versus SNR when $L = 125$ and RMSE versus sample size L when SNR is -9 dB in Fig. 4. When comparing Fig. 4 with Figs. 3 and 1, we can observe that the proposed GCB (as well as IAA) is robust to assumption of uncorrelated sources while MUSIC, R-MUSIC and SCB are not able to localize the 4 sources due to coherence. Again GCB performs the best for all SNR levels and all sample sizes L.

RMSE versus angle separation: We consider two sources ($K = 2$) with varying angle separation δ_θ. The DOA of the 1^{st} source is $\theta_1 = -30.02^o$ (off-grid) and $\theta_2 = \theta_1 + \delta_\theta$ for 2^{nd} source. The SNR is -3 dB and the sample size $L = 125$. Fig. 5 illustrates that GCB, IAA and SCB are not able to identify close-by sources as accurately as MUSIC an R-MUSIC when $\delta_\theta \leq 6^o$. GCB has better performance over IAA when $\delta_\theta \leq 7^o$ but perform on par otherwise.

V. Concluding Remarks

We proposed greedy Capon beamformer that greedily selects a high-power source using Capon SINR maximization principle and spatial power spectrum. The power of the selected source is estimated and subsequently the INCM is updated. The method is computationally light and performed favourably against SCB and some SOTA methods.

REFERENCES

[1] H. L. Van Trees, *Detection, Estimation and Modulation Theory, Part IV: Optimum Array Processing*. New York, NY, USA: Wiley, 2002, Art. no. 1456.

[2] J. Capon, "High resolution frequency-wavenumber spectral analysis," *Proc. IEEE*, vol. 57, no. 8, pp. 1408–1418, Aug. 1969.

[3] R. O. Schmidt, "Multiple emitter location and signal parameter estimation," *IEEE Trans. Antennas Propag.*, vol. AP-34, no. 3, pp. 276–280, Mar. 1986.

[4] A. Barabell, "Improving the resolution performance of eigenstructure-based direction-finding algorithms," in *Proc. IEEE Int. Conf. Acoust., Speech, Signal Process.*, 1983, pp. 336–339.

[5] Z. Yang, J. Li, P. Stoica, and L. Xie, "Sparse methods for direction-of-arrival estimation," in *Academic Press Library in Signal Processing*, vol. 7. Amsterdam, The Netherlands: Elsevier, 2018, pp. 509–581.

[6] H. Krim and M. Viberg, "Two decades of array signal processing: The parametric approach," *IEEE Signal Process. Mag.*, vol. 13, no. 4, pp. 67–94, Jul. 1996.

[7] A. M. Elbir, K. V. Mishra, S. A. Vorobyov, and R. W. Heath, "Twenty-five years of advances in beamforming: From convex and nonconvex optimization to learning techniques," *IEEE Signal Process. Mag.*, vol. 40, no. 4, pp. 118–131, Jun. 2023.

[8] A. Baggeroer and H. Cox, "Passive sonar limits upon nulling multiple moving ships with large aperture arrays," in *Proc. IEEE Conf. Rec. 33rd Asilomar Conf. Signals, Syst., Comput.*, 1999, pp. 103–108.

[9] X. Mestre and M. A. Lagunas, "Finite sample size effect on minimum variance beamformers: Optimum diagonal loading factor for large arrays," *IEEE Trans. Signal Process.*, vol. 54, no. 1, pp. 69–82, Jan. 2006.

[10] Y. I. Abramovich and N. K. Spencer, "Diagonally loaded normalised sample matrix inversion (LNSMI) for outlier-resistant adaptive filtering," in *Proc. IEEE Int. Conf. Acoust., Speech, Signal Process.*, Apr. 15–20, 2007, pp. III-1105–III-1108.

[11] L. Yang, M. R. McKay, and R. Couillet, "High-dimensional MVDR beamforming: Optimized solutions based on spiked random matrix models," *IEEE Trans. Signal Process.*, vol. 66, no. 7, pp. 1933–1947, Apr. 2018.

[12] C. D. Richmond, "Capon–Bartlett cross-spectrum and a perspective on robust adaptive filtering," *Signal Process.*, vol. 171, 2020, Art. no. 107473.

[13] D. Wipf and S. Nagarajan, "Beamforming using the relevance vector machine," in *Proc. 24th Int. Conf. Mach. Learn.*, 2007, pp. 1023–1030.

[14] P. Stoica, P. Babu, and J. Li, "SPICE: A sparse covariance-based estimation method for array processing," *IEEE Trans. Signal Process.*, vol. 59, no. 2, pp. 629–638, Feb. 2011.

[15] T. Yardibi, J. Li, P. Stoica, M. Xue, and A. B. Baggeroer, "Source localization and sensing: A nonparametric iterative adaptive approach based on weighted least squares," *IEEE Trans. Aerosp. Electron. Syst.*, vol. 46, no. 1, pp. 425–443, Jan. 2010.

[16] H. Abeida, Q. Zhang, J. Li, and N. Merabtine, "Iterative sparse asymptotic minimum variance based approaches for array processing," *IEEE Trans. Signal Process.*, vol. 61, no. 4, pp. 933–944, Feb. 2013.

[17] P. Gerstoft, C. F. Mecklenbräuker, A. Xenaki, and S. Nannuru, "Multi-snapshot sparse Bayesian learning for DOA," *IEEE Signal Process. Lett.*, vol. 23, no. 10, pp. 1469–1473, Oct. 2016.

[18] C. F. Mecklenbräuker, P. Gerstoft, E. Ollila, and Y. Park, "Robust and sparse M-estimation of DOA," *Signal Process.*, vol. 220, 2024, Art. no. 109461.

[19] E. Ollila, "Sparse signal recovery and source localization via covariance learning," 2024, *arXiv:2401.13975[stat.ME]*.

[20] Q. Wang, H. Yu, J. Li, F. Ji, and F. Chen, "Sparse Bayesian learning using generalized double Pareto prior for DOA estimation," *IEEE Signal Process. Lett.*, vol. 28, pp. 1744–1748, 2021.

[21] L. Du, J. Li, and P. Stoica, "Fully automatic computation of diagonal loading levels for robust adaptive beamforming," *IEEE Trans. Aerosp. Electron. Syst.*, vol. 46, no. 1, pp. 449–458, Jan. 2010.

[22] J. Sherman and W. J. Morrison, "Adjustment of an inverse matrix corresponding to a change in one element of a given matrix," *Ann. Math. Statist.*, vol. 21, no. 1, pp. 124–127, 1950.

[23] CGDP-SBL Software. Accessed: Jul. 27, 2024. [Online]. Available: https://github.com/WQsen/CGDP-SBL

[24] SBL Software, ver. 4.0. Accessed: Jul. 27, 2024. [Online]. Available: https://github.com/gerstoft/SBL